Journal of Global Positioning Systems (*2023*)
Vol. 19, Joint No. 1 & No. 2: 24-35
DOI: 10.5081/jgps.19.1.24

Analyzing the influence of the February 26-28th, 2023 Geomagnetic Storm on Global Ionospheric Scintillation and GPS Positioning

Shuanglei Cui[1], Xueli Zhang[1], Dongsheng Zhao[1]✉, Qianxin Wang[1], Craig M. Hancock[2], Kefei Zhang[1]

1 School of Environment and Spatial Informatics, China University of Mining and technology, Xüzhou, China

2 School of Architecture, Building and Civil Engineering, Loughborough University, United Kingdom

✉ **Corresponding author,** dszhao@cumt.edu.cn

***Abstract*:** This study examines the influence of ionospheric scintillation on GPS Precise Point Positioning (PPP) during a geomagnetic storm event that took place from February 26-28th, 2023. The analysis utilizes data from global IGS stations, as well as stations in Alaska, Canada, and Hong Kong. Findings indicate that geomagnetic storms can trigger ionospheric scintillation, leading to disruptions in GPS positioning accuracy. However, it is important to note that not all instances of ionospheric scintillation are solely attributed to geomagnetic storms; they can also arise from the interaction between charged particles and the ionosphere. During the geomagnetic storm, ionospheric scintillation primarily manifests in high-latitude regions and propagates towards lower latitudes. The impact is more pronounced in high-latitude areas, with variations observed between the northern and southern hemispheres, wherein the northern hemisphere experiences greater effects. Understanding these mechanisms is vital to ensure the precision and stability of kinematic PPP solutions obtained through GPS during geomagnetic storms.

Keywords: GPS, Geomagnetic storms, Precise Point Positioning, Ionospheric scintillation

1. Introduction

Geomagnetic storms, which follow solar activities like solar flares, coronal mass ejections, and high-speed solar wind streams, are significant disturbances in the global space environment. These storms occur when high-speed plasma clouds, generated by solar activity, reach the vicinity of Earth a few days later, causing disruptions in the Earth's magnetic field. This phenomenon is known as a geomagnetic storm (Gonzalez et al., 1994). Geomagnetic storms have a profound impact on GPS Precise Point Positioning (PPP) by amplifying and varying ionospheric delays in GPS phase and code data. This, in turn, affects high-precision GPS relative positioning (Odijk, 2001). In low-to-mid latitudes, geomagnetic storms can even cause disruptions in total electron content (TEC) and result in satellite signal loss (Astafyeva et al., 2014).

Ionospheric scintillation is closely linked to disturbances in the geomagnetic field, particularly in high-latitude regions (Jiao & Morton, 2015). Ionospheric scintillation refers to random fluctuations in the amplitude and phase of radio signals as they pass through irregularities in the ionospheric electron density (Basu & Groves, 2002). Various factors influence ionospheric scintillation, including the intensity of geomagnetic storms, storm onset time, local time, season, day-night variations, and latitude (Fuller-Rowell et al., 1994; Nava et al., 2016; Mansilla, 2019; Zhao et al., 2021). It is most commonly observed during the post-sunset hours in equatorial and polar regions during periods of heightened solar activity (Li et al., 2010; Béniguel et al., 2011; Marques et al., 2016; Veellil et al., 2020). Luo et al. (2018) conducted a study using data collected from 15 Hong Kong Satellite Positioning Reference Network stations and an ionospheric scintillation monitoring receiver between October 6th and November 17th, 2015. Their research confirmed that the Rate of TEC Index (ROTI) can serve as a reliable metric for detecting scintillation, replacing S4 and σφ. Juan et al. (2018) introduced the Along Arc TEC Rate (AATR) index to evaluate ionospheric activity across multiple solar cycles, and their findings revealed a strong correlation with ionospheric disturbances. Subsequently, Wilken et al. (2018) proposed the DIXSG index, which accurately characterizes the spatio-temporal variations of small-to-medium-scale ionospheric disturbances. They applied this index during a severe geomagnetic/ionospheric

***Editor-In-Charge*: Dr. Changsheng Cai**

storm (Saint Patrick's Day storm) on March 17th, 2015, and verified its reliability against ROTI and AATR indices. The DIXSG index exhibited a high correlation with the Dst index, making it suitable for indicating geomagnetic storm events.

During periods of scintillation, the penetration of magnetospheric electric fields into the ionosphere causes fluctuations in TEC, adversely affecting navigation systems (Basu et al., 2001). Ionospheric scintillation interferes with positioning accuracy in several ways, primarily due to range errors and satellite signal loss (cycle slips) (Basu & Groves, 2002; Conker et al., 2003; Zhang et al., 2014; Zhao et al., 2019; Luo et al., 2022). Bergeot et al. (2011) investigated the effects of GPS positioning during the Halloween storm of 2003 and identified TEC and magnetic field perturbations as contributors to degraded kinematic PPP positioning caused by second-order signal delays. Yang et al. (2015) analyzed ionospheric disturbances resulting from geomagnetic storms during the Saint Patrick's Day storm in 2015. They utilized dual-frequency carrier observations from over 5500 GNSS stations worldwide to derive kinematic PPP solutions, revealing more severe impacts in high-latitude regions and variations in PPP degradation based on different types of ionospheric disturbances in lower latitudes. Luo et al. (2018) conducted kinematic PPP positioning using the BeiDou Navigation Satellite System (BDS) during scintillation periods and found that both horizontal and vertical positioning errors had root mean square values exceeding 0.5m.

The aim of this study is to analyze the influence of Ionospheric scintillation induced by geomagnetic storms on kinematic PPP solutions using GPS. The DIXSG index will be utilized to characterize the geomagnetic storm event that occurred from February 26-28th, 2023, while the ROTI index will provide insights into ionospheric scintillation.

2. Data and Method

2.1 Station Data

This study utilized data from global IGS stations, as well as stations in Alaska, CHAIN, and Hong Kong, collected from February 26-28th, 2023. To ensure data consistency, stations that had varying data availability during the three-day period were excluded in advance, resulting in a final selection of 240 IGS stations. The station data had a sampling rate of 30 seconds, and only GPS signals were utilized in the kinematic PPP solution. Figure 1 depicts the geographical locations of all the stations employed in this study.

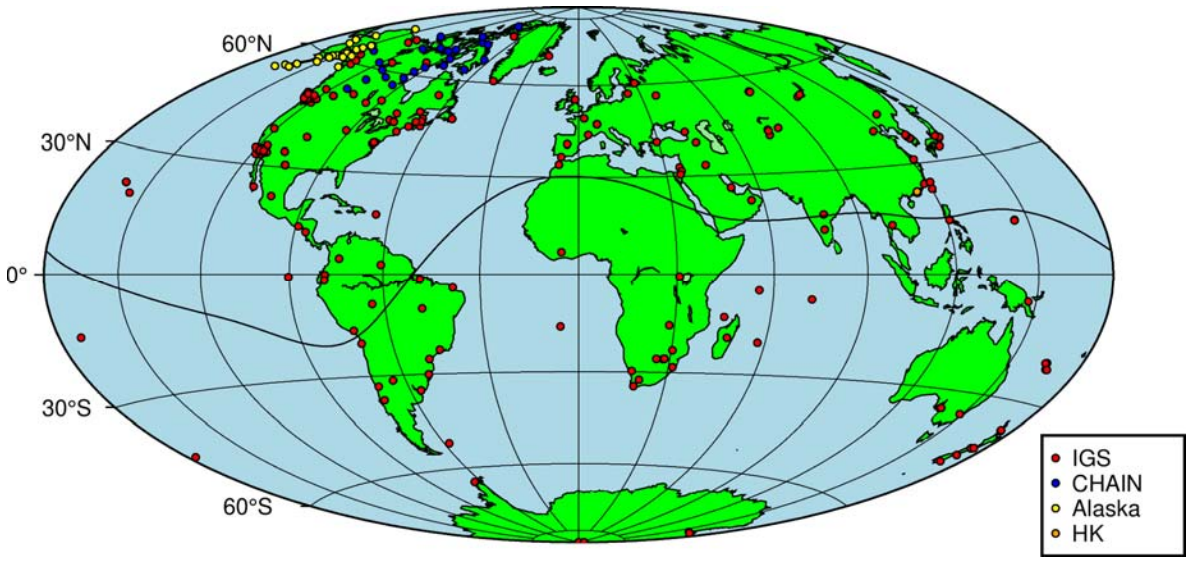

Figure 1 The geographical distribution of the stations. The solid black line indicates the magnetic equator. IGS stations are represented by the color red, Alaska stations by yellow, CHAIN stations by blue, and Hong Kong Observatory stations by orange

2.2 Disturbance Ionosphere Index Spatial Gradient (DIXSG)

The Disturbance Ionosphere Index Spatial Gradient (DIXSG) is derived from the calculation of the Disturbance Ionosphere Index (DIX) using differential GNSS carrier phase observations, building upon the research conducted by Wilken et al. (2018). Initially, the gradient variation of Slant Total Electron Content (STEC), which is weighted by the elevation angle over time, is computed as follows:

$$cROT_m^k = \left| \frac{\Delta STEC_m^k}{\Delta t \cdot \Delta s_m} \right| \quad (1)$$

Here, denotes the change in STEC between two consecutive observation arcs at a given epoch. k represents the satellite, m represents the receiver, and represents the distance between the Ionospheric Pierce Point (IPP) at a predetermined assumed ionospheric height within a specific time interval. This distance parameter helps mitigate interference caused by satellite elevation angles. Subsequently, the DIXSG is determined under a specified sensitivity level condition:

$$DIXSG(cROT_{(level)})_{i,j}^k = \left(\frac{|cROT_m^k - cROT_n^k|}{cROT_{level}}\right)^3 \left(\frac{d}{D}\right)^{-1} \quad (2)$$

Where represents the sensitivity level, n represents the receiver, d represents the distance between satellite k and the corresponding IPP for receivers m and n, and D represents the maximum permissible distance within the receiver observation network, which is typically set to 1000 km. The user has the flexibility to choose the size and number of sensitivity levels. To simplify the DIXSG under different sensitivity levels, the calculated DIXSG values are reassigned as follows:

$$DIXSG(cROT_{(level)})_{m,n}^k \geq 1 = 1 \quad (3)$$

$$DIXSG(cROT_{(level)})_{m,n}^k < 1 = 0 \quad (4)$$

Lastly, this study employs five sensitivity levels (50, 100, 150, 200, and 250) to compute the DIXSG within specific regions:

$$DIXSG_{(5-level)} = \frac{\sum_{L=1}^{5} DIXSG((cROT_{(level)}(L)))}{N} \quad (5)$$

Here, L denotes the number of sensitivity levels. The position of each DIXSG is represented by the central point of each IPP pair, and the maximum value within the selected area corresponds to the specific part of the ionosphere during a given time period (usually 1 hour). N represents the total count of valid areas, indicating the presence of at least one value within the area.

2.3 Rate of Total Electron Content Index (ROTI)

The Rate of Total Electron Content Index (ROTI), introduced by Pi et al. (1997), serves as a metric for assessing ionospheric scintillation and irregularity based on GPS dual-frequency phase observations. ROTI is calculated as the standard deviation of the Total Electron Content (TEC) rate (ROT) within a sliding window of 5 minutes (10 epochs) using GPS data sampled at a frequency of 30 seconds. To mitigate multipath effects, the elevation angle is typically set at 30°. The specific formula for ROTI calculation is as follows:

$$ROTI = \sqrt{\langle ROT^2 \rangle - \langle ROT \rangle^2} \quad (6)$$

where < • > denotes the time average within the sliding window, ROT represents the temporal derivative of Slant Total Electron Content (STEC) between two consecutive epochs. The ROT value is computed using the following equation:

$$ROT = \frac{STEC(i) - STEC(i-1)}{\Delta t} \quad (7)$$

Here, Δt represents the time interval between adjacent epochs in minutes, and i denotes the epoch. The STEC is determined using the formula:

$$STEC(i) = \frac{\phi_{L1}(i) - \phi_{L2}(i)}{40.309 \cdot 10^{16} \cdot (\frac{1}{f2^2} - \frac{1}{f1^2})} \quad (8)$$

wherein $\Phi_{L1,2}$ refers to the carrier phase observations in the L1 and L2 frequency bands, while $f1$ and $f2$ represent the frequencies in the L1 and L2 bands, respectively, with $f1$ = 1575.42 MHz and $f2$ = 1227.60 MHz.

Small-scale plasma irregularities can have a significant impact on GPS signals, resulting in scintillation effects. In this analysis, ROTI is utilized to quantify the level of ionospheric plasma density irregularities and their influence on kinematic PPP solutions throughout the study (Yang et al., 2015). Assuming a thin-shell structure at an altitude of 350 km in the ionosphere, ROTI values are subsequently mapped to the corresponding Ionospheric Pierce Points (IPPs) (Nie et al., 2022).

2.4 GPS Kinematic Precise Point Positioning (PPP) Solution

Kinematic PPP solution processing for carrier phase and pseudorange measurements was performed using the RTKLIB software (Real-Time Kinematic Library). The solution was computed with a sampling rate of 30 seconds. To mitigate the impact of multipath and ensure a sufficient number of satellites for accurate positioning, an elevation angle threshold of 10° was applied.

To achieve high-precision results in kinematic PPP, error corrections were implemented for GPS dual-frequency observations. These corrections encompassed various sources of errors, including satellite-related factors such as clock errors, orbit deviations, antenna phase offsets, and relativistic effects. Additionally, corrections were made for atmospheric errors, including ionospheric and tropospheric effects, as well as receiver-related errors such as clock biases and antenna phase center deviations. Geophysical factors like tides and Earth rotation were also taken into account during the error correction process. Table 1 describes the settings.

3. Experimental results

3.1 Geomagnetic Storm Event Description

On February 26th, a geomagnetic storm event occurred on Earth, which was influenced by a coronal mass ejection (CME) and a high-speed solar wind stream on February 24-25th, 2023. This geomagnetic storm had a prolonged duration and a significant level of disturbance, leading to ionospheric scintillation and a reduction in GPS positioning accuracy.

To evaluate the extent of disturbance caused by this geomagnetic storm, three indices, namely SYM-H, Kp, and ASY-H, were utilized to characterize the event. The SYM-H index (horizontal component asymmetry index) is computed every minute and can be regarded as a high-resolution Dst index (disturbance storm time index) (Wanliss & Showalter, 2006). The Dst index is classified into five levels: minor (-50, 30], moderate (-100, -50], strong (-200, -100], severe (-300, -200], and extreme (-∞, -300]. The Kp index (three-hourly geomagnetic index) is also divided into five levels: minor (5-, 5, 5+), moderate (6-, 6, 6+), strong (7-, 7, 7+), severe (8-, 8, 8-, 9-), and extreme (9_0). The ASY-H index (vertical component asymmetry index) is commonly employed to depict the activity level of auroras and exhibits a strong correlation with the trend of the AE index.

Table 1. Kinematic PPP Processing Strategy for GPS Dual-Frequency Ionosphere-Free Combinations

Parameters	Model and Strategy
Observations	GPS dual-frequency phase measurements
Processing Model	Forward filtering
Elevation Angle Threshold	10°
Sampling Interval	30s
Cycle Slip Detection	GF and MW detection (TurboEdit)
Satellite Orbits	IGS final precise orbits with a sampling interval of 15min
Satellite Clocks	IGS final clock products with a sampling interval of 30s
Phase Center Offset	igs08.atx
Ionospheric Delay	Ionosphere-free model
Tropospheric Delay	ZTD estimation
Differential Code Bias	Chinese Academy of Sciences rapid correction product
Solid Earth Tides	Model correction
Relativistic Effects	Model correction
Earth Rotation	Earth rotation parameters provided by IGS

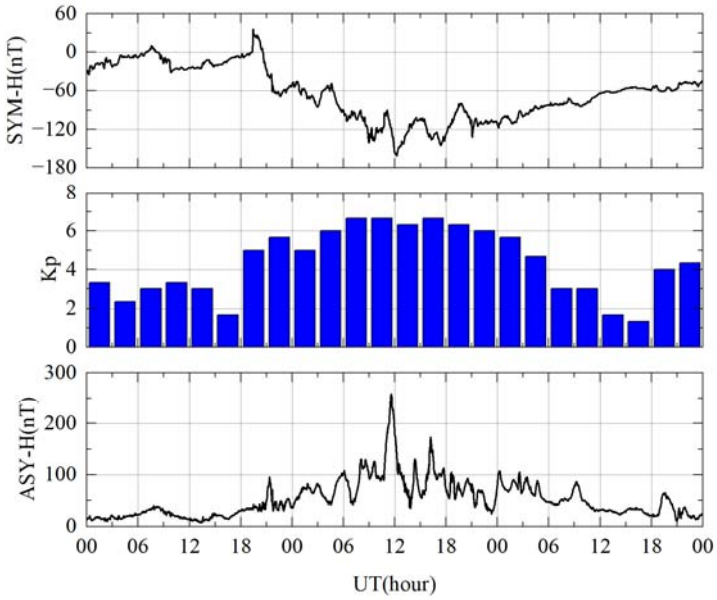

Figure 2 Geomagnetic index from Ferbruary 26-28th, 2023

Figure 2 illustrates the geomagnetic indices, SYM-H and Kp, during the period from February 26-28th, 2023. The ASY-H index is used as a substitute for the AE index. The geomagnetic storm was predominantly observed on the 27th, known as the main phase, with the initial phase starting at 20:00 on the 26th and the recovery phase beginning on the 28th, lasting for several days. The storm reached its peak at 12:00 on the 27th, with the minimum value of SYM-H reaching -161nT and the Kp index peaking at 6.67. This event can be categorized as a strong geomagnetic storm.

Figures 3, 4, and 5 present the Dst index for the period of February 26-28th, 2023, along with the DIXSG indices for three regions: Alaska, Canada, and Hong Kong. The DIXSG index is computed using the Δs weighting factor, which is larger at lower elevation angles and gradually decreases as the elevation angles increase. The figures demonstrate a strong correlation between the DIXSG index and the Dst index. However, as a regional index, the DIXSG index is expected to offer a more accurate reflection of the geomagnetic storm level in the specific region compared to the global Dst index. By examining the DIXSG index, it is apparent that Alaska reached a peak state between 0:00 and 20:00 on the 27th, Hong Kong experienced peak periods from 10:00 to 15:00 and from 21:00 on the 27th to 3:00 on the 28th, while Canada did not exhibit a distinct peak in the DIXSG index. The subsequent sections will provide a detailed description of the relationship between the DIXSG index and positioning accuracy.

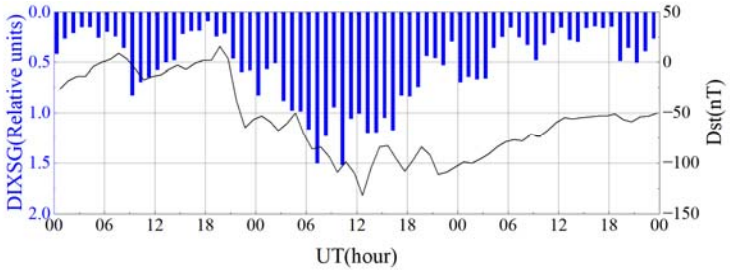

Figure 3. DIXSG index (blue) and Dst index (black) in the Alaska from February 26-28th, 2023

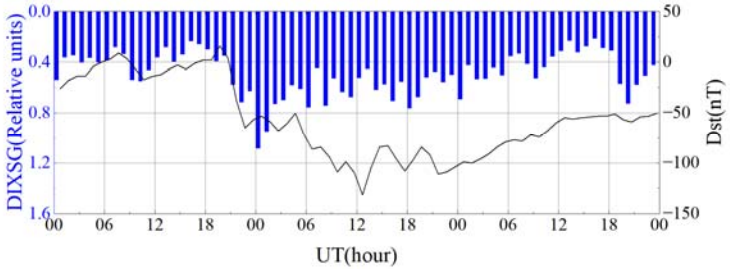

Figure 4. DIXSG index (blue) and Dst index (black) in Canada from February 26-28th, 2023

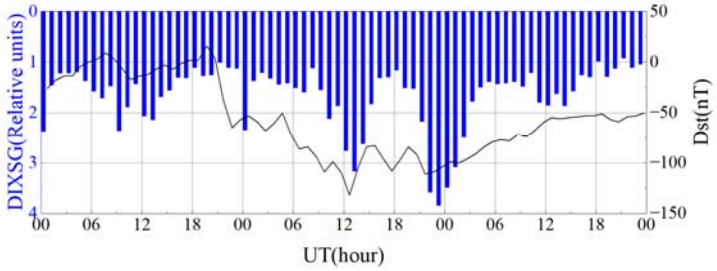

Figure 5. DIXSG index (blue) and Dst index (black) in Hong Kong from February 26 -28th, 2023

3.2 Analysis of the impact of global ionospheric scintillation on Kinematic PPP errors

Figures 6 and 7 depict spatiotemporal maps with a 4-hour resolution, illustrating the variations in the Rate of TEC Index (ROTI) and dynamic Precise Point Positioning (PPP) errors for all stations between 18:00 on February 26th and 14:00 on February 28th, 2023. The blue shading represents nighttime, while the solid black line represents the magnetic equator. The IGS stations are denoted by circles, Alaska stations by diamonds, CHAIN stations by stars, and Hong Kong Observation Network stations by pentagons. Analyzing

the figures, it is evident that prior to the occurrence of the geomagnetic storm at 18:00 on the 26th, the ionosphere, as indicated by ROTI, was predominantly calm. With a few exceptions, the positioning accuracy remained within 0.1m. Notably, ionospheric scintillation occurred near the magnetic equator, resulting in decreased positioning accuracy of two stations in that region, exceeding 0.5m and lasting for a certain duration. This phenomenon aligns with the characteristics of Equatorial Plasma Irregularities (EPI) after sunset (Wan et al., 2021). At 20:00, the geomagnetic storm entered its initial phase, causing disruptions of varying types, degrees, and geographical locations in the ionosphere due to geomagnetic activity. By 22:00, the storm phase was in effect. In high-latitude regions of North America, ROTI values were absent due to a 30° elevation angle threshold setting. This was a consequence of poor observation quality at the time, resulting in fewer available observations for ROTI calculations. However, ionospheric scintillation persisted in this area, and the positioning accuracy of North American stations deteriorated significantly, with positioning errors mostly exceeding 0.5m. In low-latitude regions, positioning errors for several stations ranged from 0.15m to 0.30m. From 22:00 on February 26th to 6:00 on February 28th, the primary mid-to-high-latitude regions (40°-90°) and low-latitude regions near the magnetic equator experienced the influence of the geomagnetic storm (Basu et al., 2002). By 14:00 on the 28th, the recovery phase of the geomagnetic storm had commenced, and the ionosphere reached a relatively calm state. Only a few stations were affected, and the positioning accuracy had returned to a precision level in the centimeter range.

The 4-hour resolution spatiotemporal maps provide an overview of the general characteristics and trends in ionospheric behavior and positioning impact during the geomagnetic storm. However, they lack the ability to capture specific details. To address this limitation, this study generated dynamic maps with a 10-minute resolution. S1 illustrates the global spatiotemporal variations of the Rate of TEC Index (ROTI), while S2 displays the global spatiotemporal variations of Precise Point Positioning (PPP) errors. Analysis of S1 and S2 reveals that the geomagnetic storm primarily influenced the ionosphere and positioning in the northern hemisphere. Through the geomagnetic storm event, the ionosphere and positioning accuracy in Antarctica and North America (40-90°) consistently experienced the effects. Numerous stations encountered compromised positioning accuracy, which can be attributed to the expansion of the auroral oval following intensified particle precipitation in regions with strong ionospheric irregularities. This phenomenon had a significant impact on positioning accuracy (Yang, 2015). In contrast, the ionospheric scintillation caused by the storm was less prominent in low-latitude regions. During the geomagnetic storm, ionospheric scintillation and the decrease in dynamic PPP accuracy occurred simultaneously, albeit with varying degrees of impact at different times during the storm. Detailed explanations will be provided based on the 10-minute resolution spatiotemporal maps of ROTI and PPP 3D RMS.

Starting from 20:00 on the 26th, ionospheric scintillation began to spread from high latitudes to mid-latitudes in North America, accompanied by an increase in the number of stations exhibiting positioning errors exceeding 0.5m. Between 22:00 on the 26th and 7:00 on the 27th, ionospheric scintillation and deteriorated positioning accuracy were observed near the geomagnetic equator. Scintillation near the geomagnetic equator and in low-latitude and mid-latitude regions predominantly occurred during the night and gradually subsided as the night progressed (Veellil et al., 2020). From 20:00 on the 26th to 7:00 on the 27th, the geomagnetic storm primarily impacted the geomagnetic equator and the Northern Hemisphere, displaying a trend of spreading from high latitudes to low latitudes. This trend can be attributed to Joule heating in high-latitude regions, which elevates the temperature of the upper atmosphere and drives the extension of the ionospheric storm from high to mid-low latitudes (Fuller-Rowell et al., 1994).

Between 7:00 and 9:30, the ionosphere near the geomagnetic equator and the positioning accuracy of stations returned to normal levels. During the peak moment of the geomagnetic storm (11:00 to 15:00), significant ionospheric scintillation occurred in Antarctica, above North America (40-90°), Hong Kong and its vicinity, Europe, and the eastern part of Australia. Between 11:00 and 13:00, over 70% of the stations above North America experienced positioning errors exceeding 0.5m, with the degradation of positioning accuracy lasting longer in the Hong Kong area. After the mitigation of ionospheric scintillation in the Hong Kong area, the North American region remained under the influence of the geomagnetic storm for an extended period, while other regions remained relatively calm until 20:00 on the 27th, when another episode of ionospheric scintillation occurred in the vicinity of Hong Kong. This continued until 4:00 on the 28th. Between 22:00 on the 27th and 4:00 on the 28th, positioning accuracy in the Hong Kong area and its neighboring stations deteriorated.

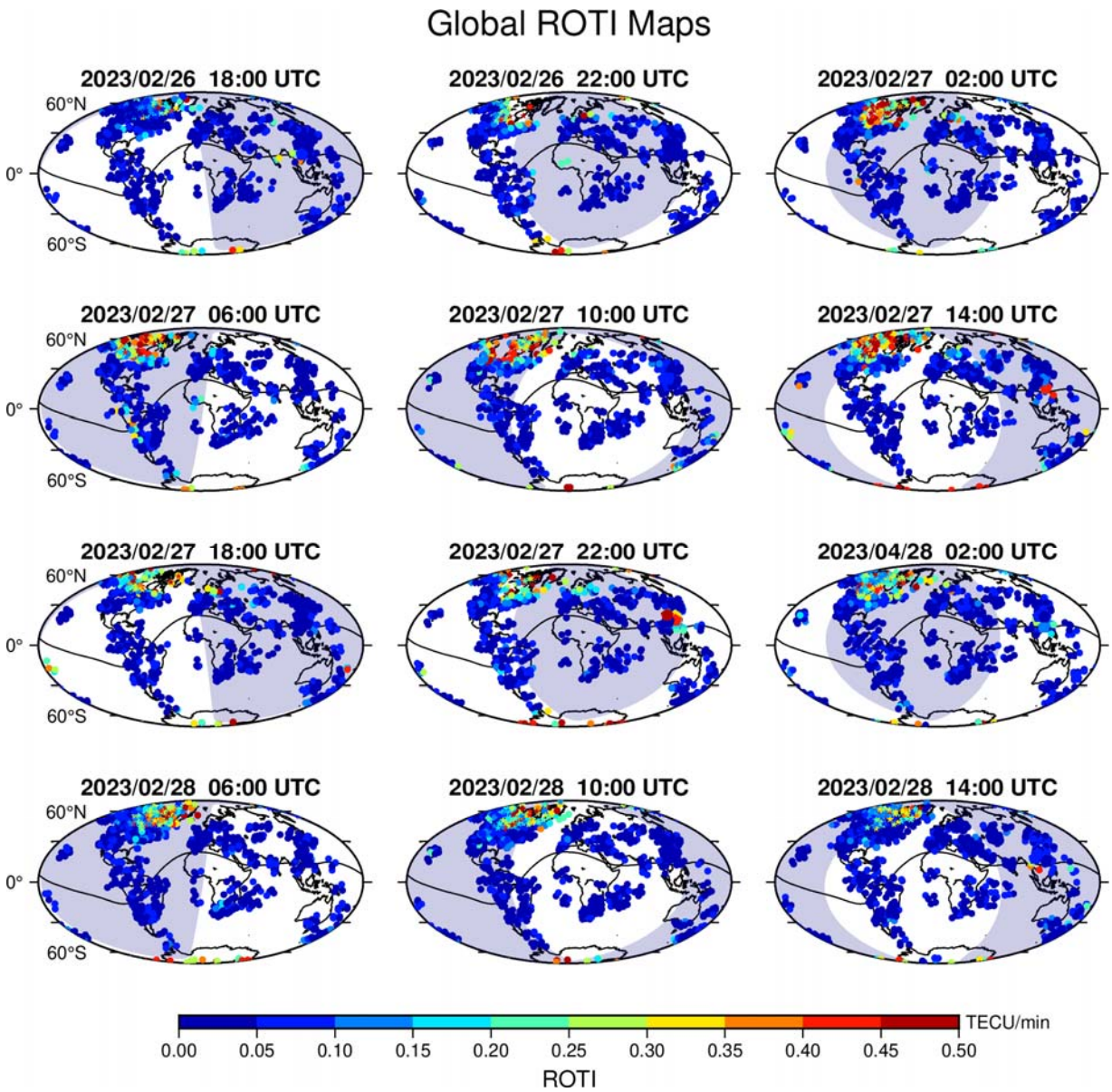

Figure 6. The global variations of ROTI (Rate of Total Electron Content Index) from February 26th, 18:00 to February 28th, 14:00, with a resolution of 4 hours. The blue shading represents nighttime, while the solid black line represents the geomagnetic equator. Circles denote IGS stations, diamonds represent Alaska stations, stars indicate CHAIN observation network, and pentagons represent the Hong Kong observation network

From 6:00 to 7:00 on the 28th, most global stations achieved normal centimeter-level positioning accuracy. However, after 7:00, some North American stations began to experience degradation in positioning accuracy. By 10:30 on the 28th, ROTI values had significantly decreased, and ROTI values in the high-latitude regions of the Northern Hemisphere were mostly within the normal range of 0.2-0.3. This phenomenon can be explained by complex particle precipitation in high-latitude regions (Juan et al., 2018). Although there were still mild scintillations, the positioning accuracy for most stations worldwide (excluding a few CHAIN stations in North America) had returned to normal levels. The geomagnetic storm was in the recovery phase, with minimal impact on the ionosphere and positioning accuracy, indicating the return to normal geomagnetic activity levels and subsequent recovery of the ionosphere and positioning accuracy.

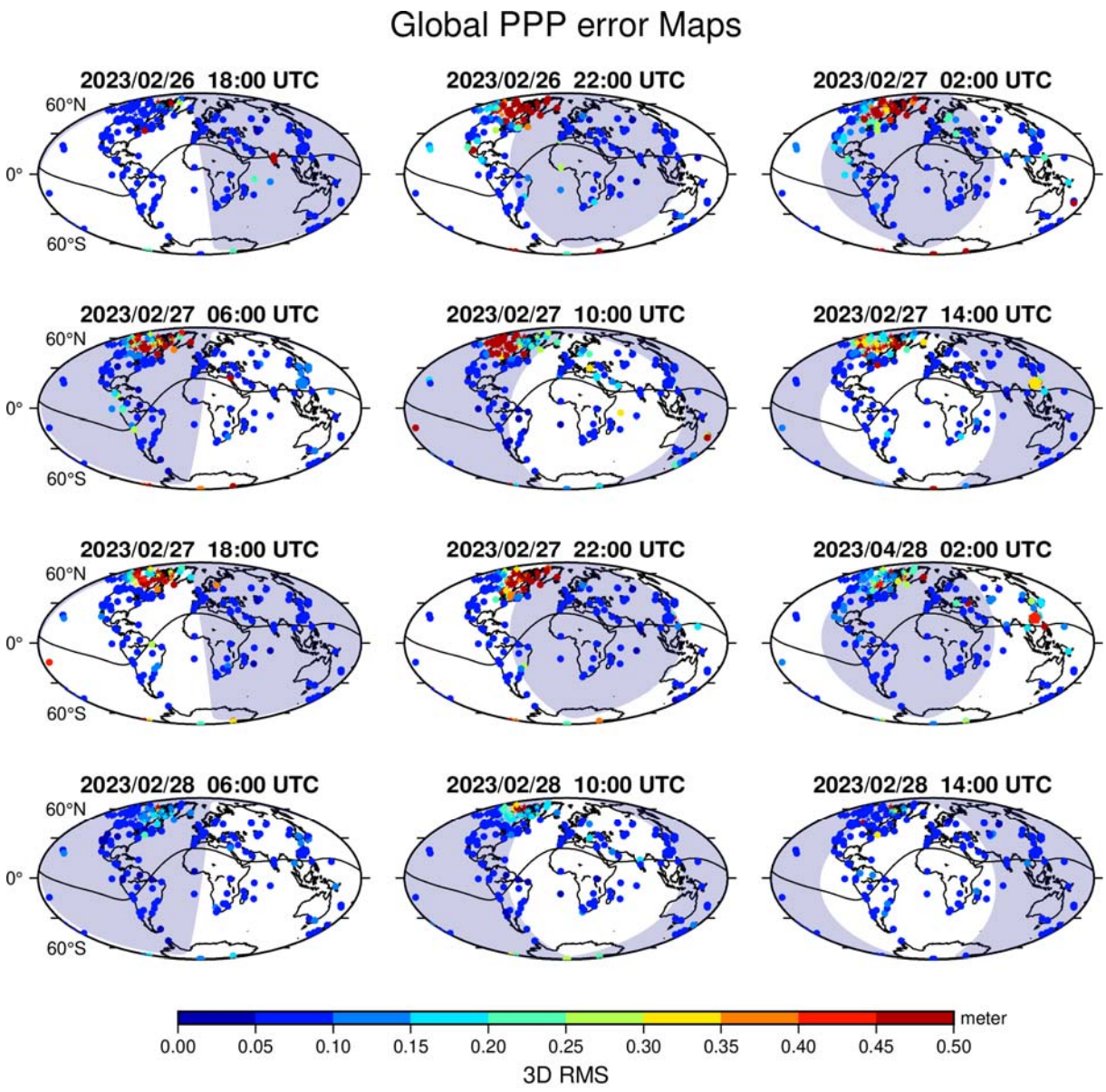

Figure 7. The global variations of 3D RMS (Root Mean Square) error in kinematic PPP (Precise Point Positioning) worldwide from February 26th, 18:00, to February 28th, 14:00, with a resolution of 4 hours. The blue shading indicates nighttime, while the solid black line represents the geomagnetic equator. IGS stations are represented by circles, Alaska stations by diamonds, the CHAIN observation network by stars, and the Hong Kong observation network by pentagons

3.3 Analysis of the Impact of Regional Geomagnetic Storm on Ionospheric Scintillation and Kinematic PPP Errors

In Alaska, the DIXSG index peaked from 0:00 to 20:00 on the 27th (Figure 3). During this period, ionospheric scintillation was observed in the Alaska region (S1), and the station's positioning accuracy was suboptimal, with most stations experiencing positioning errors exceeding 0.5m (S2). Additionally, ROTI indicated the occurrence of ionospheric scintillation in Alaska from 22:00 on the 27th to 3:00 on the 28th (during the second scintillation period in the Hong Kong region). However, unlike the previous case, this ionospheric scintillation did not affect positioning accuracy.

From S1, it can be observed that ionospheric scintillation occurred in the Hong Kong region during two periods: 11:00 to 15:00 on the 27th and 20:00 on the 27th to 4:00 on the 28th. The DIXSG index in Figure 5 also reflects a peak period in the Hong Kong region during the geomagnetic storm. Not only did the data from the 18 stations in the Hong Kong observation network indicate increased ROTI values and decreased positioning accuracy, but several nearby stations also

exhibited similar behavior. Due to the close proximity of the Hong Kong stations, their characteristics cannot be observed on a global map. Therefore, separate spatio-temporal maps of kinematic PPP errors with a 1-hour resolution (Figure 8 and Figure 9) and positioning errors with a 10-minute resolution in the Hong Kong region (S3) were generated. From Figure 8, Figure 9, and S3, it is evident that the first scintillation event in Hong Kong was significantly more severe than the second event. At its peak, the positioning accuracy of all 18 stations deteriorated to over 0.5m. As the 18 stations are closely located, the impact of the geomagnetic storm on their positioning is similar. It can be inferred that the influence of the geomagnetic storm on ionospheric scintillation and positioning accuracy is regional and affects a specific range.

For the CHAIN stations, it can be observed from S1 and S2 that they experienced the most severe impact on the ionosphere and positioning accuracy. Even at 14:00 on the 28th, when the positioning accuracy of most stations had returned to normal levels, several CHAIN stations still had positioning errors exceeding 0.5m. However, the DIXSG index in this region did not exhibit a clear peak and had relatively small values. The reason for this could be that ionospheric scintillation in this area is not solely caused by the geomagnetic storm but rather by the interaction of charged particles in the auroral oval region descending along the Earth's magnetic field into the polar region atmosphere and colliding with atoms and molecules in the upper atmosphere, resulting in coupling effects with the ionosphere.

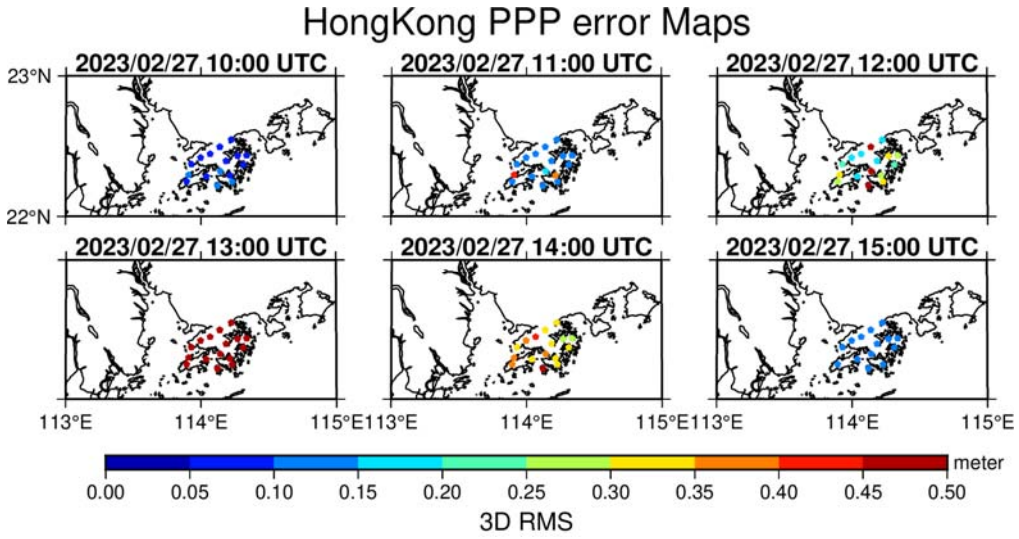

Figure 8. Global PPP 3D RMS variations maps from 10:00 to 15:00 on February 27, 2023 (1-hour resolution)

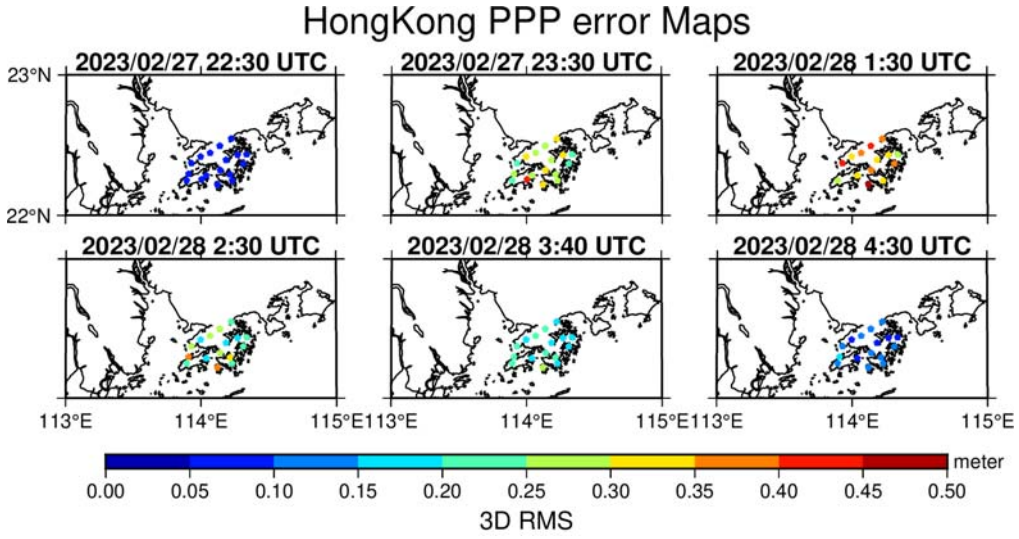

Figure 9 Global PPP 3D RMS variations maps from 22:30 on February 27, 2023 to 4:30 on February 28, 2023 (1-hour resolution). Since the PPP is the convergence time at 0:30 on the 28th, it is skipped

4 Conclusions

This study investigated the effects of ionospheric scintillation caused by a geomagnetic storm on kinematic PPP GPS positioning. Global IGS stations and three regional stations were analyzed for the period from February 26-28th, 2023. ROTI and DIXSG indices were utilized to assess the irregularities in plasma density induced by the storm. The findings highlight the following key points:

(1) Geomagnetic storms induce ionospheric scintillation, leading to degradation in positioning accuracy and potential loss of lock. However, it should be noted that not all ionospheric scintillation is directly linked to geomagnetic storms. Scintillation observed in the Canadian region, for example, is attributed to the interaction between charged particles and the ionosphere. During intense geomagnetic storms, ROTI values indicate heightened levels of ionospheric scintillation, resulting in positioning errors exceeding 0.5m for the majority of stations.

(2) The impact of geomagnetic storms is significantly more pronounced in the Northern Hemisphere compared to the Southern Hemisphere, with North America (40-90°) experiencing particularly severe effects. Ionospheric scintillation typically initiates in high-latitude regions of North America and propagates towards lower latitudes. During the recovery phase of a geomagnetic storm, high-latitude stations are the last to regain normal positioning accuracy.

(3) Geomagnetic storms predominantly affect high-latitude and equatorial regions in terms of ionospheric scintillation and positioning accuracy. Among these regions, high-latitude areas endure more severe consequences, including a higher number of affected stations, larger positioning errors, and longer durations of impact. In high-latitude regions, positioning errors frequently exceed 0.5m, while in equatorial regions, errors range from 0.15m to 0.5m.

(4) The DIXSG index exhibits a correlation with the Dst index, indicating the occurrence of geomagnetic storms and ionospheric scintillation. During the degradation phase of positioning accuracy in Hong Kong and Alaska stations, the DIXSG index reaches its peak.

(5) The impact of geomagnetic storms demonstrates regional characteristics, with stations within a specific region experiencing comparable levels of influence on positioning accuracy.

Data Acquisition

SYM-H, Kp, ASY-H, and Dst data were obtained from the World Data Center for Geomagnetism, Kyoto (https://wdc.kugi.kyoto-u.ac.jp/). IGS station data were acquired from the National Aeronautics and Space Administration (https://cddis.nasa.gov/). Alaska station data were sourced from the Earth Scope Consortium (https://observablehq.com/). CHAIN station data were obtained from the Canadian High Arctic Ionospheric Network (http://chain.physics.unb.ca/). Hong Kong data were collected from the Hong Kong Geodetic Survey Services (https://www.geodetic.gov.hk/).

Acknowledgments

This research was supported by National Natural Science Foundations of China (Nos. 42204016; 42274021), the Natural Science Foundation of Jiangsu Province (No. BK20200664), State Key Laboratory of Geo-Information Engineering (No. SKLGIE2021-M-2-1), the Construction Program of Space-Air-Ground-Well Cooperative Awareness Spatial Information Project (No. B20046) and the Jiangsu Dual Creative Doctors Project.

References

Astafyeva E, Yasyukevich Y, Maksikov A, Zhivetiev I (2014): Geomagnetic storms, super-storms, and their impacts on GPS-based navigation systems. Space Weather 12(7):508– 525.

Basu S, Basu Sa, Valladares CE, Yeh HC, Su SY, MacKenzie E, Sultan PJ, Aarons J, Rich FJ, Doherty P, Groves KM, Bullett TW (2001): Ionospheric effects of major magnetic storms during the International Space Weather Period of September and October 1999: GPS observations, VHF/UHF scintillations, and in situ density structures at middle and equatorial latitudes. Journal of Geophysical Research 106(A12):30389– 30413.

Basu S, Groves KM, Basu Su, Sultan PJ (2002): Specification and forecasting of scintillations in communication navigation links: current status and future plans. Journal of Atmospheric and Solar-Terrestrial Physics 64(16):1745-1754.

Basu S & Groves KM (2002): Specification and Forecasting of Outages on Satellite Communication and Navigation Systems. Geophysical Monograph Series 125:423-430.

Bergeot N, Bruyninx C, Defraigne P, Pireaux S,Legrand J,Pottiaux E, Baire Q (2011): Impact of the Halloween 2003 ionospheric storm on kinematic GPS positioning in Europe. GPS Solutions 15(2):171–180 .

Béniguel Y, Adam JP, Bourdillon A, Lassudrie-Duchesne P (2011): Ionosphere scintillation effects on navigation systems. Comptes Rendus Physique 12(2):186–191.

Conker RS, El-Arini MB, Hegarty CJ, Hsiao T (2003): Modeling the effects of ionospheric scintillation on GPS/Satellite-based augmentation system availability. Radio Science 38(1):1–23.

Fuller-Rowell TJ, Codrescu MV, Moffett RJ, Quegan S (1994): Response of the thermosphere and ionosphere to geomagnetic storms. Journal of Geophysical Research 99(A3): 3893 – 3914.

Gonzalez WD, Joselyn JA, Kamide Y, Kroehl HW, Rostoker G, Tsurutani BT, Vasyliunas VM (1994): What is a geomagnetic storm?.Journal of Geophysical Research 99(A4):5771– 5792.

Jakowski N, Stankov S, Schlueter S, Klaehn D (2006): On developing a new ionospheric perturbation index for space weather operations. Advances in Space Research 38(11): 2596–2600.

Jakowski N, Borries C, Wilken V (2012): Introducing a disturbance ionosphere index. Radio Science 47(4): RS0L14.

Jiao Y & Morton YT (2015): Comparison of the effect of high-latitude and equatorial ionospheric scintillation on GPS signals during the maximum of solar cycle 24. Radio Science 50(9):886– 903.

Juan JM, Sanz J, Rovira-Garcia A, González-Casado G,Ibáñez D, Orus Perez R (2018): AATR an ionospheric activity indicator specifically based on GNSS measurements. Journal of Space Weather and Space Climate 8(A14):11.

Li G, Ning B, Ren Z,Hu L (2010): Statistics of GPS ionospheric scintillation and irregularities over polar regions at solar minimum. GPS Solutions 14(4):331–341.

Luo X, Lou Y, Xiao Q, Gu S, Chen B, Liu Z. (2018): Investigation of ionospheric scintillation effects on BDS precise point positioning at low-latitude regions. GPS Solutions 22(3): 63.

Luo X, Du J, Lou Y, Gu S, Yue X, Liu J, Chen B (2022): A method to mitigate the effects of strong geomagnetic storm on GNSS precise point positioning. Space Weather 20(1): e2021SW002908.

Mansilla GA (2019): Behavior of the Total Electron Content over the Arctic and Antarctic sectors during several intense geomagnetic storms. Geodesy and Geodynamics 10(1):26-36.

Marques HAS, Monico JFG, Marques HA (2016): Performance of the L2C civil GPS signal under various ionospheric scintillation effects. GPS Solutions 20(2):139–149.

Nava B, Rodríguez-Zuluaga J, Alazo-Cuartas K, Kashcheyev A, Migoya-Orué Y, Radicella SM, Amory-Mazaudier C, Fleury R (2016): Middle- and low-latitude ionosphere response to 2015 St. Patrick's Day geomagnetic storm. Journal of Geophysical Research: Space Physics 121(4):3421 – 3438.

Nie W, Rovira-Garcia A, Wang Y, Zheng D, Yan L, Xu T (2022): On the global kinematic positioning variations during the September 2017 solar flare events. Journal of Geophysical Research: Space Physics 127(8): e2021JA030245.

Odijk D (2001): Instantaneous Precise GPS Positioning under Geomagnetic Storm Conditions.GPS Solutions 5(2):29–42.

Pi X, Mannucci A, Lindqwister U, Ho C (1997): Monitoring of global ionospheric irregularities using the worldwide GPS network. Geophysical Research Letters 24(18):2283–2286.

Vadakke Veettil S, Aquino M, Marques HAm, Moraes A (2020): Mitigation of ionospheric scintillation effects on GNSS precise point positioning (PPP) at low latitudes. Journal of Geodesy 94(2):15.

Wanliss JA, Showalter KM, (2006): High-resolution global storm index: Dst versus SYM-H. Journal of Geophysical Research 111(A2): A02202.

Wan X, Xiong C, Gao, S, Huang F, Liu Y, Aa E, Yin F, Cai H (2021): The nighttime ionospheric response and occurrence of equatorial plasma irregularities during geomagnetic storms: a case study. Satellite Navigation 2(1):23.

Wilken V, Kriegel M, Jakowski N, Berdermann J (2018): An ionospheric index suitable for estimating the degree of ionospheric perturbations.Journal of Space Weather and Space Climate 8(A19):9.

Yang Z, Morton YTJ, Zakharenkova I, Cherniak I, Song S, Li W (2020): Global view of ionospheric disturbance impacts on kinematic GPS positioning solutions during the 2015 St. Patrick's Day storm. Journal Of Geophysical Research: Space Physics 125(7): e2019JA027681.

Zhang X, Guo F, Zhou P (2014): Improved precise point positioning in the presence of ionospheric scintillation. GPS Solutions 18(1):51–60.

Zhao D, Hancock CM, Roberts GW, Jin S (2019): Cycle Slip Detection during High Ionospheric Activities Based on Combined Triple-Frequency GNSS Signals. Remote sensing 11(3):250.

Zhao D, Wang L, Wang Q, Liu X, Li C, Hancock C, Roberts GW, Zhang K (2022): Statistical Study on the Characterization of Phase and Amplitude Scintillation Events in the High-latitude Region During 2014-2020 Based on ISMR. Advances in Space Research 69(9):3435-3459.

Authors

Shuanglei Cui is currently a master student at China University of Mining and Technology. His research interest is ionospheric scintillation monitoring.

Xueli Zhang is currently a master student at China University of Mining and Technology. His research interest is ionospheric scintillation monitoring.

Dongsheng Zhao is an associate professor at the School of Environment and Spatial Informatics, China University of Mining and Technology. He received his Ph.D. and B.Eng degrees from the University of Nottingham and Wuhan University, respectively. His current research interests focus on GNSS remote sensing, particularly in ionospheric scintillation monitoring and modeling.

Qianxin Wang is a Professor and the vice-dean at the School of Environment and Spatial Informatics, China University of Mining and Technology. He received his Ph.D. degree from Central South University, China. His current research interests include geodetic data processing and satellite positioning.

Craig M. Hancock is a Reader in surveying at the School of Architecture, Building and Civil Engineering, Loughborough University. He obtained his Ph.D. degree from Newcastle University and worked in the University of Nottingham for 14 years. His research interests are GNSS error source modeling, BIM and digital construction.

Kefei Zhang is a Professor at the School of Environment and Spatial Informatics, China University of Mining and Technology. He received his Ph.D. degree from Curtin University, Australia. His research interests include GNSS atmospheric modeling, space mining and precision agriculture.